PONTIFICIA UNIVERSIDAD CATÓLICA DE CHILE
ESCUELA DE INGENIERÍA

A MIXED-INTEGER DISTRIBUTION NETWORK PLANNING MODEL USING A TIGHT POWER FLOW RELAXATION

NICOLÁS EDUARDO LOBOS RODRÍGUEZ

Thesis submitted to the Office of Research and Graduate Studies
in partial fulfillment of the requirements for the degree of
Master of Science in Engineering

Advisor:
MATÍAS NEGRETE-PINCETIC

Santiago de Chile, September 2018

PONTIFICIA UNIVERSIDAD CATÓLICA DE CHILE
ESCUELA DE INGENIERÍA

A MIXED-INTEGER DISTRIBUTION NETWORK PLANNING MODEL USING A TIGHT POWER FLOW RELAXATION

NICOLÁS EDUARDO LOBOS RODRÍGUEZ

Members of the Committee:
MATÍAS NEGRETE-PINCETIC
ÁLVARO LORCA GÁLVEZ
DANIEL OLIVARES QUERO
FELIPE FEIJÓO PALACIOS
DIEGO LÓPEZ-GARCÍA

Thesis submitted to the Office of Research and Graduate Studies
in partial fulfillment of the requirements for the degree of
Master of Science in Engineering

Santiago de Chile, September 2018

A mis Padres y Abuelos

AGRADECIMIENTOS

A muchas personas debo el haber podido desarrollar todo el trabajo de tesis que aquí presento, y más importante aún, el camino que recorrí para llegar a su fin. Mis más sinceros agradecimientos a mis profesores Álvaro, Daniel y Matías, quienes me guiaron y apoyaron a lo largo de estos dos años, y a quienes hoy también considero como unos muy buenos amigos.

En esta etapa de mi vida tuve la suerte de conocer a personas increíbles junto a las cuales he crecido y aprendido innumerables cosas. Gracias Pablo, Matías, Juan Carlos, Enrique, Rodrigo, Alan, Fred, Samuel, Pablo B., Benjamín, Rodrigo H., George, Pablo G., Felipe, Cristian, Altamiro, Marcelo, Tomás, Leo y a toda la familia del Laboratorio de Optimización, Control y Mercados de Energía, de la que espero formar parte por el resto de mi vida. En ustedes no veo compañeros de universidad ni colegas de la profesión, sino que verdaderos amigos que espero conservar y acompañar a lo largo de sus vidas, victorias y derrotas. Para todos ustedes, espero que sepan que siempre podrán contar conmigo.

Gracias a mi familia, quienes me apoyaron y motivaron a lo largo de todo este recorrido. Gracias Yasna, por tu amor y compañia, por estar allí y decir siempre lo que hacía falta escuchar. Gracias sobre todo a tí mamá, papá y lela, sin todo su amor, cariño y cuidado, no sería la persona ni mucho menos el profesional en que me he vuelto gracias a ustedes. Y a mis abuelitos, que me acompañan ahora y siempre. Los amo a todos ustedes con todo mi corazón.

Finalmente, rescato una frase que mi amigo Matías destacó en una de sus lecturas, y que hoy para mi hace más sentido que nunca.

"*Don't be deceived by life's outcomes. Life's outcomes, while not entirely random, have a huge amount of luck baked into them. Above all, recognize that if you have had*

success, you have also had luck and with luck comes obligation. You owe a debt, and not just to your Gods. You owe a debt to the unlucky." (Michael Lewis, 2012).

Gracias a todos, a los que estuvieron, a quienes están, y a quienes no tuvieron la oportunidad.

TABLE OF CONTENTS

LIST OF FIGURES

LIST OF TABLES

ABSTRACT

This thesis presents a mixed-integer optimization model for the distribution network planning problem. The model considers important aspects including investments in feeders, substations, and distributed generation (DG), as well as power imports, over a given planning horizon. The main feature of this model is that it accurately represents the physics of power flows through the use of a tight polyhedral relaxation, based on a known outer approximation of the second-order cone. An extensive set of computational experiments show the value of the proposed approach for understanding the effects of DG integration, the effectiveness of the relaxation employed, and the computational efficiency of the overall planning model.

Keywords: Distributed generation, distribution network planning, mixed-integer optimization, optimal power flow.

RESUMEN

Este trabajo de tesis presenta un modelo de optimización entera-mixta para abordar el problema de planificación de la distribución. El modelo desarrollado considera múltiples aspectos, incluyendo inversiones en alimentadores, subestaciones, y generación distribuida (GD), así como las importaciones de energía desde el sistema eléctrico troncal sobre un horizonte de planificación determinado. La principal característica de este modelo es que representa de forma precisa la fenomenología de los flujos de potencia a través de una relajación poliedral de las ecuaciones del flujo de potencia, basada en una conocida aproximación exterior del cono de segundo orden. Una serie de experimentos computacionales muestra el valor del enfoque propuesto para entender los efectos de la integración de GD, la efectividad del modelo de flujos de potencia empleado, y la eficiencia computacional del modelo de planificación en general.

Palabras Clave: Flujo óptimo de potencia, generación distribuida, optimización entera-mixta, planificación de la distribución.

1. INTRODUCTION

1.1. Context

In recent years, the surge in the integration of distributed energy resources (DERs) has exposed a series of benefits, issues, and challenges that push the need for new and effective distribution network planning (DNP) tools. The DNP problem consists of determining how to expand a distribution network (DN) throughout a given planning horizon. A very important challenge associated with this problem consists of properly modelling DER alternatives and other technical aspects, while at the same time, representing the power flow equations in a precise but tractable form. The aim of this thesis is to address this challenge.

1.2. Distributed Energy Resources

The integration of DERs, implies several benefits. As presented in Figure 1.1, DERs are easily installed almost anywhere in a DN, due to their modularity and size. Due to this, DERs foster the development of new electricity market structures (e.g. local energy markets) and the response to changing market conditions, Pepermans et al. (2005). They can also help reduce load requirements and power losses, improve voltage profiles and reliability, and support load management, El-Khattam & Salama (2004). Furthermore, DERs can significantly help limiting green house gas emissions as they can displace fossil-fuel based generation. Various smart grid concepts can exploit DERs to even displace the need for large power plants, helping to reduce some investments, Pudjianto et al. (2007). However, the surge of DERs integration entails several technical challenges such as reverse power flows and loss of protection effectiveness, voltage regulation, a lack of output predictability from DG, and reactive power issues, that may reduce the security and the power quality, Paliwal et al. (2014). Therefore, further considerations into the DNP problem become critical to exploit the opportunities of DERs while overcoming these challenges.

For a comprehensive review on aspects related to major benefits, issues and challenges of DERs integration refer to Keane et al. (2013).

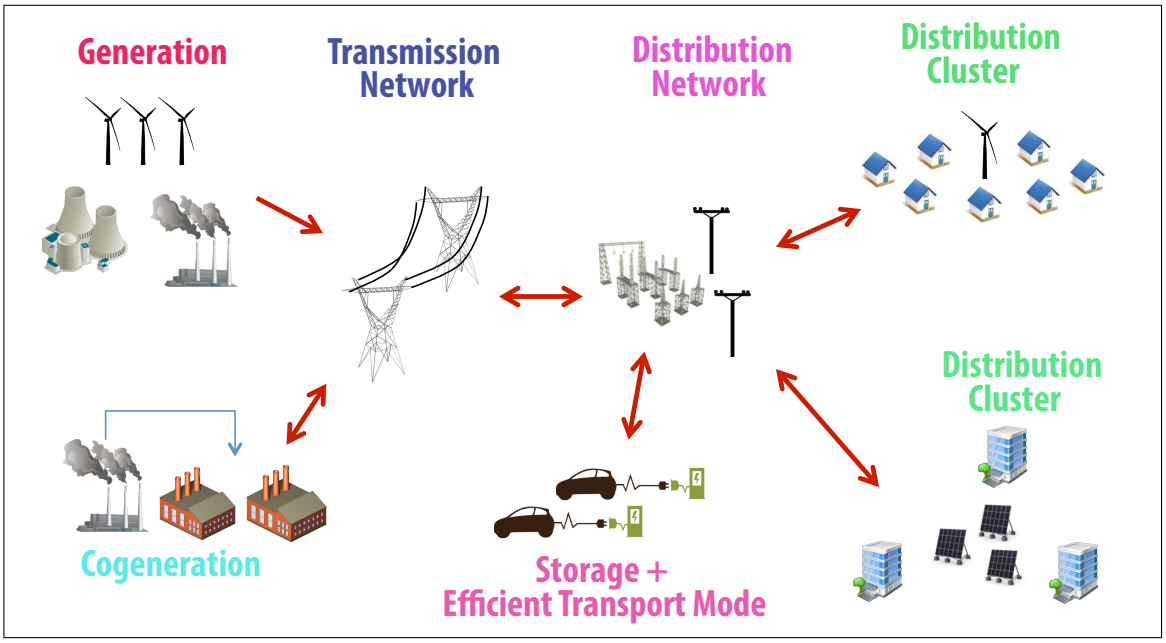

Figure 1.1. Power Systems Structure

1.3. The Distribution Network Planning Problem

The DNP involves a large number of alternatives to consider, such as the allocation, sizing and timing within a planning horizon of new investments and subsequent expansions in capacity of feeders, substations, DG units, capacitor banks, voltage regulators and price-dependent DERs such as battery energy storage systems and demand response programs, while considering a certain physical representation of power flows and topological constraints, among other possible features.

Some major difficulties in modelling the DNP are not only the scale of the problem, given the number of elements at DNs that ultimately entails the need for both binary and continuous decision variables, but also the representation of the power flow equations in an effective and tractable form. On the one hand, it would be ideal to employ AC-OPF

equations, however, their non-convexity makes this a major difficulty. On the other hand, a simple approximation of AC-OPF, such as the classic DC-OPF representation, is not well suited to DNs due to their incapability to capture relevant physical aspects such as high power losses, and voltage and thermal limits.

Due to these difficulties, the DNP has been tackled in various ways. Some approaches have directly considered AC-OPF constraints at the expense of using meta-heuristic optimization algorithms, as in Ziari et al. (2013), Zeng et al. (2014) and Koutsoukis et al. (2018), which are capable of treating non-convexities, but they are unable to ensure closeness to global optimality. Meanwhile, some other works have managed to formulate linear and mixed-integer models, which can ensure the quality of the solutions obtained in terms of closeness of global optimality at expense of a representation of the physical system. However, many of the existing approaches obviate the complexity in the power flow equations, using various simplifications such as using only Kirchhoff's current and voltage laws and ignoring other aspects, as is the case of Gönen & Foote (1981), Haffner et al. (2008b), Haffner et al. (2008a), Muñoz-Delgado et al. (2015), Shen et al. (2017), Asensio et al. (2016b), and Asensio et al. (2016a). Instead, some other approaches make use of linearizations that require estimated operational points, Tabares et al. (2016), or use strong assumptions regarding voltage magnitudes and bus angle differences that may no longer apply in some distribution systems (e.g. rural systems), Alotaibi & Salama (2018). For a comprehensive review on different techniques involved in solving the DNP, refer to Prakash & Khatod (2016) and Theo et al. (2017).

1.4. Representation of the Power Flows

Fortunately, in order to address the difficulties associated with the non-convexities in AC-OPF, several effective approximations and convex relaxations have been developed. The work in Coffrin & Van Hentenryck (2014) presents a linear approximation of the

AC-OPF that improves over some of the limitations of DC-OPF. Also, the existent relaxations of AC-OPF include convex quadratic relaxations, Coffrin et al. (2016), semidefinite programming (SDP) relaxations, Bai et al. (2008), Lavaei & Low (2012), Kocuk et al. (2016a), and second-order cone programming (SOCP) relaxations, R. A. Jabr (2006), R. A. Jabr (2008), Kocuk et al. (2016b), Kocuk et al. (2017). A particular advantage of SOCP relaxations is their practical computational tractability. See Low (2014a) and Low (2014b) for a thorough survey in this matter.

Another interesting development in previous years is the development of linear relaxations of SOCP problems. The seminal work of Ben-Tal and Nemirovski Ben-Tal & Nemirovski (2001) developed a highly efficient and accurate linear relaxation for such problems. This idea has been employed in various applications, such as solving general mixed-integer SOCP problems, Vielma et al. (2008), and approximating quadratic generation costs in OPF problems, R. Jabr (2012).

1.5. Main Contributions

In this thesis, we present an effective mixed-integer optimization model for the DNP problem where we leverage the recent progress in convex relaxations of AC-OPF. The proposed model considers several technical aspects including investments in feeders, substations, and DG. The proposed model also considers multiple investment periods, while operational dynamics are represented through load blocks. Further, the proposed model considers special constraints that ensures that the DN maintains a radial topology. The power flow model employed is based on the SOCP relaxation of AC-OPF and the linear relaxation of SOCP problems developed by Ben-Tal and Nemirovski Ben-Tal & Nemirovski (2001), resulting in a very tight linear relaxation of the power flow equations. With this, the model accurately represents power flow phenomena, considering physical power flow elements such as voltages and reactive power flows.

The main contributions of this work are summarized as follows:

(i) Application of an SOCP relaxation of the AC-OPF problem and a subsequent linear relaxation to effectively capture the physics of power flows in the context of DNP problems.

(ii) Development of a mixed-integer optimization model for the DNP problem that includes investments and upgrades in feeders, substations and DG integration, while appropriately modelling power flow equations. The model also implements a series of physical validity constraints that speed-up the solution process.

(iii) Assessment of the performance of the proposed DNP model to understand the effects of DG integration, the effectiveness of the power flow model employed, and the computational efficiency of the overall planning model.

1.6. Document Organization

The rest of the document is organized as follows. Section 2 presents the nomenclature needed to fully understand the proposed mixed-integer optimization model for the DNP problem. Section 3 presents the OPF model employed. Section 4 presents the DNP problem formulation. Section 5 presents various computational experiments. Finally, Section 6 provides concluding remarks.

2. NOMENCLATURE

2.1. Sets and Indexes

$u \in \mathcal{U}$**:**	Index and set of planning stages.
$t \in \mathcal{T}$**:**	Index and set of temporal blocks.
$i \in \mathcal{B}$**:**	Index and set of buses.
$\mathcal{G} \subset \mathcal{B}$**:**	Set of generation buses.
$\mathcal{S} \subset \mathcal{G}$**:**	Set of substation buses.
$\mathcal{DG} \subset \mathcal{G}$**:**	Set of DG cluster buses.
$ij \in \mathcal{L}$**:**	Index and set of lines.
$\delta(i) \subset \mathcal{B}$**:**	Set of neighbour buses of bus i.
$\Upsilon(u) \subset \mathcal{B}$**:**	Set of transfer node buses at stage u.

2.2. Parameters

$\bar{c}_{ij}^{nf}$**:**	Fixed cost of installing a new feeder (US$/km).
$\bar{c}_{ij}^{rf}$**:**	Fixed cost of reinforcing an existing feeder (US$/km).
$\tilde{c}_{ij}^{nf}$**:**	Variable capacity cost in a new feeder (US$/MVA·km).
$\tilde{c}_{ij}^{rf}$**:**	Variable capacity cost in a reinforced feeder (US$/MVA·km).
$\bar{c}_{i}^{ns}$**:**	Fixed cost of installing a new substation (US$).
$\bar{c}_{i}^{rs}$**:**	Fixed cost of reinforcing an existing substation (US$).
$\tilde{c}_{i}^{ns}$**:**	Variable capacity cost in a new substation (US$/MVA).
$\tilde{c}_{i}^{rs}$**:**	Variable capacity cost in a reinforced substation (US$/MVA).
$\tilde{c}_{i}^{dg}$**:**	DG investment cost (US$/MVA).
$o_{i,t}^{s}$**:**	Supply cost at substations (US$/MWh).
$\upsilon_{i,t}^{sh}$**:**	Unserved energy cost (US$/MWh).
h_t**:**	Number of hours of load block t in any given year.
r^d**:**	Annual discount rate.

r^c: Capital recovery factor.

y_u: Number of chronological years in any investment period.

τ^e: Life time of project e.

$\phi_{i,t}$: DG capacity factor.

$\underline{V}_i$: Minimum voltage magnitude.

$\overline{V}_i$: Maximum voltage magnitude.

ψ_i^d: Load power factor at each node.

$n(\mathcal{B})$: Number of buses.

$n(\mathcal{B}^s)$: Number of substation buses.

α: Maximum proportion of the minimum load level at each bus for DG integration.

β: Maximum proportion of the minimum load level of the entire DN for DG integration.

$\rho_{ij}^{nf,\textbf{min}}$: Minimum capacity associated to a new candidate feeder (MVA).

$\rho_{ij}^{nf,\textbf{max}}$: Maximum capacity associated to a new candidate feeder (MVA).

$\rho_{ij}^{rf,\textbf{min}}$: Minimum capacity associated to a reinforced existing feeder (MVA).

$\rho_{ij}^{rf,\textbf{max}}$: Maximum capacity associated to a reinforced existing feeder (MVA).

$\sigma_i^{ns,\textbf{min}}$: Minimum capacity associated to a new candidate substation (MVA).

$\sigma_i^{ns,\textbf{max}}$: Maximum capacity associated to a new candidate substation (MVA).

$\sigma_i^{rs,\textbf{min}}$: Minimum capacity associated to a reinforced existing substation (MVA).

$\sigma_i^{rs,\textbf{max}}$: Maximum capacity associated to a reinforced existing substation (MVA).

$\varphi_i^{dg,\textbf{max}}$: Maximum DG integration capacity (MVA).

2.3. Decision Variables

$x_{ij,u}^{nf}$: Binary decision for installing a new feeder.

$x_{ij,u}^{rf}$: Binary decision for reinforcing an existing feeder.

$\rho_{ij,u}^{nf}$: Capacity installed in a new feeder (MVA).

$\rho^{rf}_{ij,u}$:	Capacity reinforcement of an existing feeder (MVA).
$z^{ns}_{i,u}$:	Binary decision for installing a new substation.
$z^{rs}_{i,u}$:	Binary decision for reinforcing an existing substation.
$\sigma^{ns}_{i,u}$:	Capacity installed in a new substation (MVA).
$\sigma^{rs}_{i,u}$:	Capacity reinforcement of an existing substation (MVA).
$\varphi^{dg}_{i,u}$:	Capacity installed in a DG cluster (MVA).
$p^{s}_{i,u,t}$:	Active (MVA) power supplied by a substation.
$q^{s}_{i,u,t}$:	Reactive (MVAr) power supplied by a substation.
$p^{dg}_{i,u,t}$:	Active (MVA) power generated by a DG cluster.
$q^{dg}_{i,u,t}$:	Reactive (MVAr) power generated by a DG cluster.
$p^{sh}_{i,u,t}$:	Active (MVA) load shedding at each node.
$q^{sh}_{i,u,t}$:	Reactive (MVAr) load shedding at each node.
$c_{ii,u,t}$:	Voltage magnitude.
$c_{ij,u,t}$:	Cosine voltage relation between connected buses i and j.
$s_{ij,u,t}$:	Sine voltage relation between connected buses i and j.
$\xi_{ij,u,t}$:	Auxiliary variable associated to the linear relaxation of the relation between connected buses.
$Y_{i,u}$:	Binary decision for making use of a transfer node.
$\mathcal{K}_{i,u}$:	Fictitious nodal demand.
$\kappa_{ij,u}$:	Fictitious flow.

3. OPTIMAL POWER FLOW MODELS

This Section presents the OPF models that will be employed in the DNP model proposed in this thesis. Consider a power network $\mathcal{N} = (\mathcal{B}, \mathcal{L})$, where generation assets are connected to a subset of buses, denoted as $\mathcal{G} \subset \mathcal{B}$. Let Y denote the admittance matrix of components $Y_{ij} = G_{ij} + iB_{ij}$ for each line $ij \in \mathcal{L}$. Additionally, it is assumed that $G_{ii} = g_{ii} - \sum_{j \neq i} G_{ij}$ and $B_{ii} = b_{ii} - \sum_{j \neq i} B_{ij}$, where g_{ii} and b_{ii} correspond to the shunt conductance and susceptance at bus i, respectively. This assumption neglects shunt capacitance of lines, and therefore these are represented only by their series impedance, which is usually the case of short distribution network power lines. Also, let p_i^g, q_i^g (p_i^ℓ and q_i^ℓ) be the real and reactive power injection of all generation assets (load) at bus i, and function $C_i(p_i^g)$ be their corresponding operational costs. Finally, consider $c_{ij} = |V_i||V_j| \cos \theta_{ij}$ and $s_{ij} = -|V_i||V_j| \sin \theta_{ij}$, for neighbour connected buses i and j. Here $|V_i|$ is the voltage magnitude of the complex voltage phasor V_i at bus i, and θ_{ij} the corresponding angular difference.

We will first present an exact equivalent formulation of the AC-OPF problem in Section 3.1. Then, in Section 3.2, we will show the SOCP-OPF relaxation of the AC-OPF. Finally, we will present a tight polyhedral relaxation of the SOCP-OPF, namely, the LP-OPF, in Section 3.3.

3.1. The Cosine-Sine Formulation of AC-OPF

Model 1 presents a full AC-OPF model (see Kocuk et al. (2016b) for details on the validity of this formulation).

Model 1: AC-OPF

$$\min \sum_{i \in \mathcal{G}} C_i(p_i^g) \tag{3.1}$$

$$\text{s.t. } p_i^g - p_i^\ell = g_{ii}c_{ii} + \sum_{j \in \delta(i)} p_{ij} \qquad \forall i \in \mathcal{B} \tag{3.2}$$

$$q_i^g - q_i^\ell = -b_{ii}c_{ii} + \sum_{j \in \delta(i)} q_{ij} \qquad \forall i \in \mathcal{B} \tag{3.3}$$

$$p_{ij} = -G_{ij}c_{ii} + G_{ij}c_{ij} - B_{ij}s_{ij} \qquad \forall ij \in \mathcal{L} \tag{3.4}$$

$$q_{ij} = B_{ij}c_{ii} - G_{ij}c_{ij} - G_{ij}s_{ij} \qquad \forall ij \in \mathcal{L} \tag{3.5}$$

$$\underline{V}_i^2 \leq c_{ii} \leq \overline{V}_i^2 \qquad \forall i \in \mathcal{B} \tag{3.6}$$

$$c_{ij} = c_{ji} \qquad \forall ij \in \mathcal{L} \tag{3.7}$$

$$s_{ij} = -s_{ji} \qquad \forall ij \in \mathcal{L} \tag{3.8}$$

$$c_{ij}^2 + s_{ij}^2 = c_{ii}c_{jj} \qquad \forall ij \in \mathcal{L} \tag{3.9}$$

$$\theta_{ji} = \text{atan2}(s_{ij}, c_{ij}) \qquad \forall ij \in \mathcal{L} \tag{3.10}$$

$$p_{ij}^2 + q_{ij}^2 \leq (S_{ij}^{\max})^2 \qquad \forall ij \in \mathcal{L} \tag{3.11}$$

$$p_i^{\min} \leq p_i^g \leq p_i^{\max} \qquad \forall i \in \mathcal{G} \tag{3.12}$$

$$q_i^{\min} \leq q_i^g \leq q_i^{\max} \qquad \forall i \in \mathcal{G} \tag{3.13}$$

The objective function in (3.1) represents total operational cost. Constraints (3.2) and (3.3) define power balance, while equations (3.4) and (3.5) represent the power flow (p_{ij}, q_{ij}) through each line. Boundaries in (3.6) limit the minimum $\underline{V}_i$ and maximum $\overline{V}_i$ voltage magnitude at each bus, while equations (3.7)–(3.10) guarantee the consistency of the presented formulation. Expression (3.11) represents transmission line flow limits

$S_{ij}^{\max}$. Finally, equations (3.12) and (3.13) determine the minimum ($p_i^{\min}, q_i^{\min}$) and maximum ($p_i^{\max}, q_i^{\max}$) active and reactive power injection of all generation means at each bus, respectively.

3.2. The SOCP-OPF

In Model 1, both equations (3.9) and (3.10) are sources of non-convexity. On the one hand, in the case of radial networks, which is typically the case in distribution systems, equation (3.10) is guaranteed to be satisfied. Thus, by dropping this constraint we still get an exact equivalent of problem (3.1)–(3.13) under radial networks (and a relaxation for meshed networks). On the other hand, the non-convex coupling constraint (3.9) can be relaxed into an SOCP constraint. Thus, with these two changes, we obtain an SOCP relaxation of AC-OPF, presented in Model 2, from Kocuk et al. (2016b).

Model 2: SOCP-OPF

$$\min \sum_{i \in \mathcal{G}} C_i(p_i^g) \tag{3.14}$$

$$\text{s.t. } c_{ij}^2 + s_{ij}^2 \leq c_{ii} c_{jj} \qquad \forall ij \in \mathcal{L} \tag{3.15}$$

$$\text{(3.2)–(3.8), (3.11)–(3.13).} \tag{3.16}$$

3.3. The LP-OPF

The SOCP-OPF is convex, which guarantees that a global optimum to such model can be obtained efficiently. Nevertheless, that model is still non-linear. Therefore, if we use SOCP-OPF in the DNP problem, we would obtain a very difficult mixed-integer SOCP problem due to the need of binary variables.

In SOCP-OPF, equations (3.11) and (3.15) can be shown to be special cases of constraints based on Lorentz cones L^k, where

$$\mathrm{L}^k = \left\{ (y_1, \ldots, y_{k+1}) \middle| \sqrt{y_1^2 + \ldots + y_k^2} \leq y_{k+1} \right\} \tag{3.17}$$

The transmission line flow limit constraints in (3.11) can be presented as the following Lorentz cone L^2 set for all lines:

$$\left(p_{ij}, q_{ij}, S_{ij}^{\max}\right) \in \mathrm{L}^2 \qquad \forall ij \in \mathcal{L} \tag{3.18}$$

Additionally, it can be seen that equation (3.15) can be expressed as the following SOCP constraint:

$$c_{ij}^2 + s_{ij}^2 + \left(\frac{c_{ii} - c_{jj}}{2}\right)^2 \leq \left(\frac{c_{ii} + c_{jj}}{2}\right)^2 \qquad \forall ij \in \mathcal{L} \tag{3.19}$$

Also, note that c_{ii} and c_{jj} are positive. Thus, equation (3.19) is equivalent to a Lorentz cone in L^3 and, based on the approach in Ben-Tal & Nemirovski (2001), (3.19) can be further represented through the following two L^2 based constraints:

$$\left(c_{ij}, s_{ij}, \zeta_{ij}\right) \in \mathrm{L}^2 \qquad \forall ij \in \mathcal{L} \tag{3.20}$$

$$\left(\zeta_{ij}, \frac{c_{ii} - c_{jj}}{2}, \frac{c_{ii} + c_{jj}}{2}\right) \in \mathrm{L}^2 \qquad \forall ij \in \mathcal{L} \tag{3.21}$$

Here, ζ_{ij} is a new auxiliary variable for each line (i, j).

By writing (3.19) using two L^2 cones is that it is possible to exploit a very effective linear relaxation of the L^2 cone developed in Ben-Tal & Nemirovski (2001). Denote such linear relaxation of $(x, y, z) \in \mathrm{L}^2$ as $\mathcal{P}^{\nu}\left(x, y, z, \boldsymbol{\mu}\right) \geq 0$. Where ν is a parameter that determines the tightness of the relaxation, and $\boldsymbol{\mu}$ is a vector of additional auxiliary variables. The detailed formulation of this relaxation is presented in Appendix A.

With the above analysis, we obtain the LP-OPF as a linear relaxation of the SOCP-OPF (3.14)–(3.16) as follows:

Model 3: LP-OPF

$$\min \sum_{i \in \mathcal{G}} C_i(p_i^g) \tag{3.22}$$

$$\text{s.t. } \mathcal{P}^{\nu^\alpha}\left(c_{ij}, s_{ij}, \zeta_{ij}, \boldsymbol{\mu_{ij}^{\alpha}}\right) \geq 0 \tag{3.23}$$

$$\mathcal{P}^{\nu^\beta}\left(\zeta_{ij}, \frac{c_{ii} - c_{jj}}{2}, \frac{c_{ii} + c_{jj}}{2}, \boldsymbol{\mu_{ij}^{\beta}}\right) \geq 0 \tag{3.24}$$

$$\mathcal{P}^{\nu^\gamma}\left(p_{ij}, q_{ij}, S_{ij}^{\max}, \boldsymbol{\mu_{ij}^{\gamma}}\right) \geq 0 \tag{3.25}$$

$$\text{(3.2)–(3.8), (3.12)–(3.13).} \tag{3.26}$$

Thus, LP-OPF (3.22)–(3.26) is also a relaxation of AC-OPF in Model 1. Depending on the tightness of the SOCP-OPF in Model 2 and the tightness of the linear relaxation of the L^2 cone, LP-OPF can also be a very tight relaxation. In what follows, this relaxation will be used as foundation of the proposed DNP problem.

4. THE DISTRIBUTION NETWORK PLANNING PROBLEM

This Section presents the DNP problem developed in this thesis. The proposed DNP involves a large number of alternatives to consider, binary and continuous decision variables determine the allocation, sizing and timing of new investments and subsequent expansions in capacity of feeders, substations, DG clusters, while considering a certain physical representation of power flows and topological constraints, among other possible features. Consider a planning horizon divided into multiple investment periods $u \in \mathcal{U}$, each of which considers different load blocks $t \in \mathcal{T}$.

4.1. Objective Function

The objective function of the proposed model aims to minimize the total investment and operational costs of the DN over the planning horizon.

$$\min \sum_{u \in \mathcal{U}} r_u^d \big(\mathcal{C}_u^f + \mathcal{C}_u^s + \mathcal{C}_u^{dg} + \mathcal{O}_u \big) \tag{4.1}$$

Where the investment costs in feeders $\mathcal{C}_u^f$, substations $\mathcal{C}_u^s$, DG clusters $\mathcal{C}_u^{dg}$, and the operational costs $\mathcal{O}_u^s$ for every stage u in the planning horizon, are defined as follows:

$$\mathcal{C}_u^f = \sum_{(i,j) \in \mathcal{L}} r^{c,f} \left(\bar{c}_{ij}^{nf} x_{ij,u}^{nf} + \tilde{c}_{ij}^{nf} \rho_{ij,u}^{nf} + \bar{c}_{ij}^{rf} x_{ij,u}^{rf} + \tilde{c}_{ij}^{rf} \rho_{ij,u}^{rf} \right) \tag{4.2}$$

$$\mathcal{C}_u^s = \sum_{i \in \mathcal{S}} r^{c,s} \left(\bar{c}_i^{ns} z_{i,u}^{ns} + \tilde{c}_i^{ns} \sigma_{i,u}^{ns} + \bar{c}_i^{rs} z_{i,u}^{rs} + \tilde{c}_i^{rs} \sigma_{i,u}^{rs} \right) \tag{4.3}$$

$$\mathcal{C}_u^{dg} = \sum_{i \in \mathcal{DG}} r^{c,dg} \tilde{c}_i^{dg} \varphi_{i,u}^{dg} \tag{4.4}$$

$$\mathcal{O}_u = \sum_{t \in \mathcal{T}} h_t \Big(\sum_{i \in \mathcal{S}} o_{i,t}^s p_{i,u,t}^s + \sum_{i \in \mathcal{B}} \upsilon_{i,t}^{sh} p_{i,u,t}^{sh} \Big) \tag{4.5}$$

Here, h_t corresponds to the number of hours of load block t in any given year.

Investment decisions are taken in stages u, each of which represents a set of chronological years. The discount factors r_u^d consider the annual discount rate r^d and y_u chronological years in a representative investment period as in (4.6). Additionally, investment costs for all projects consider a capital recovery factor $r^{c,e}$ as in (4.7), for every transmission, generation and DG cluster e. The total investment cost is annualized for a given weighted average capital cost using a capital recovery factor r^c and the respective life time of the project τ^e.

$$r_u^d = \frac{1}{(1+r^d)^{y_u(u-1)}} \sum_{i=1}^{y_u} \frac{1}{(1+r^d)^{(i-1)}} \tag{4.6}$$

$$r^{c,e} = \frac{r^c}{1-(1+r^c)^{-\tau^e}} \tag{4.7}$$

4.2. Optimal Power Flow Constraints

The active and reactive power flow balance at each node considers power injections and withdrawals from all energy sources and loads as presented in (4.8) and (4.9).

$$p_{i,u,t}^s + p_{i,u,t}^{dg} - p_{i,u,t}^{\ell} + p_{i,u,t}^{sh} = g_{ii}c_{ii,u,t} + \sum_{j\in\delta(i)} p_{ij,u,t} \qquad \forall i \in \mathcal{B}, u \in \mathcal{U}, t \in \mathcal{T} \tag{4.8}$$

$$q_{i,u,t}^s + q_{i,u,t}^{dg} - q_{i,u,t}^{\ell} + q_{i,u,t}^{sh} = -b_{ii}c_{ii,u,t} + \sum_{j\in\delta(i)} q_{ij,u,t} \qquad \forall i \in \mathcal{B}, u \in \mathcal{U}, t \in \mathcal{T} \tag{4.9}$$

The active and reactive power flows through each line are defined through Big-M type constraints (4.10) and (4.11). Additional bounds (4.12) and (4.13) negate power flows through non-existent lines.

$$|p_{ij,u,t} + G_{ij}c_{ii,u,t} - G_{ij}c_{ij,u,t} + B_{ij}s_{ij,u,t}| \leq \mathrm{M}(1-x_{ij,u}^{nf}) \;\; \forall ij \in \mathcal{L}, u \in \mathcal{U}, t \in \mathcal{T} \tag{4.10}$$

$$|q_{ij,u,t} - B_{ij}c_{ii,u,t} + G_{ij}c_{ij,u,t} + G_{ij}s_{ij,u,t}| \leq \mathrm{M}(1-x_{ij,u}^{nf}) \;\; \forall ij \in \mathcal{L}, u \in \mathcal{U}, t \in \mathcal{T} \tag{4.11}$$

$$|p_{ij,u,t}| \leq \mathrm{M}x_{ij,u}^{nf} \qquad \forall ij \in \mathcal{L}, u \in \mathcal{U}, t \in \mathcal{T} \tag{4.12}$$

$$|q_{ij,u,t}| \leq \mathrm{M}x_{ij,u}^{nf} \qquad \forall ij \in \mathcal{L}, u \in \mathcal{U}, t \in \mathcal{T} \tag{4.13}$$

The following equations bound the voltage magnitude of all buses in (4.14), and relate the cosine and sine variables for all the pairs of buses connected through each existent and candidate line as in equations (4.15) and (4.16). In particular, equations (4.17) and (4.18) determine the polyhedral approximation of the SOCP cone formulation of equations (3.23) and (3.24), namely as in the LP-OPF. All the Big-M inequalities in these constraints become active in case a transmission corridor is installed between the corresponding buses.

$$\underline{V}_i^2 \leq c_{ii,u,t} \leq \overline{V}_i^2 \qquad \forall i \in \mathcal{B}, u \in \mathcal{U}, t \in \mathcal{T} \tag{4.14}$$

$$|c_{ij,u,t} - c_{ji,u,t}| \leq \mathrm{M}(1 - x_{ij,u}^{nf}) \qquad \forall i \in \mathcal{B}, u \in \mathcal{U}, t \in \mathcal{T} \tag{4.15}$$

$$|s_{ij,u,t} + s_{ji,u,t}| \leq \mathrm{M}(1 - x_{ij,u}^{nf}) \qquad \forall i \in \mathcal{B}, u \in \mathcal{U}, t \in \mathcal{T} \tag{4.16}$$

$$\mathcal{P}^{\nu^\alpha}\left(c_{ij,u,t}, s_{ij,u,t}, \xi_{ij,u,t}, \boldsymbol{\mu}_{\boldsymbol{ij,u,t}}^{\boldsymbol{\alpha}}\right) \geq 0 \qquad \forall i \in \mathcal{B}, u \in \mathcal{U}, t \in \mathcal{T} \tag{4.17}$$

$$\mathcal{P}^{\nu^\beta}\left(\xi_{ij,u,t}, \frac{c_{ii,u,t} - c_{jj,u,t}}{2}, \frac{c_{ii,u,t} + c_{jj,u,t}}{2} + \mathrm{M}(1 - x_{ij,u}^{nf}), \boldsymbol{\mu}_{\boldsymbol{ij,u,t}}^{\boldsymbol{\beta}}\right) \geq 0 \qquad \forall i \in \mathcal{B}, u \in \mathcal{U}, t \in \mathcal{T} \tag{4.18}$$

Similarly to equation (3.25), transmission line flow limit constraints for each corridor are defined as a system of linear inequalities as in (4.19), where the transmission limit $\rho_{ij,u}^{nf} + \rho_{ij,u}^{rf}$ corresponds to the sum of the initially invested and the latter reinforced capacities.

$$\mathcal{P}^{\nu^\gamma}\left(p_{ij,u,t}, q_{ij,u,t}, \rho_{ij,u}^{nf} + \rho_{ij,u}^{rf}, \boldsymbol{\mu}_{\boldsymbol{ij,u,t}}^{\boldsymbol{\gamma}}\right) \geq 0 \qquad \forall ij \in \mathcal{L}, u \in \mathcal{U}, t \in \mathcal{T} \tag{4.19}$$

Substations active and reactive power supply limitations consider both the initially invested and the latter reinforced capacities as in equations (4.20) and (4.21). The active and reactive power generation from DG clusters are limited by the total installed capacity and the generation capacity factor at each bus and load level $\phi_{i,t}$ as in (4.22) and (4.23).

$$p_{i,u,t}^s \leq \sigma_{ij,u}^{nf} + \sigma_{ij,u}^{rf} \qquad \forall i \in \mathcal{S}, u \in \mathcal{U}, t \in \mathcal{T} \tag{4.20}$$

$$|q_{i,u,t}^s| \leq \sigma_{ij,u}^{nf} + \sigma_{ij,u}^{rf} \qquad \forall i \in \mathcal{S}, u \in \mathcal{U}, t \in \mathcal{T} \tag{4.21}$$

$$p^{dg}_{i,u,t} \leq \phi_{i,t}\varphi^{dg}_{i,u} \qquad \forall i \in \mathcal{DG}, u \in \mathcal{U}, t \in \mathcal{T} \tag{4.22}$$

$$|q^{dg}_{i,u,t}| \leq \phi_{i,t}\varphi^{dg}_{i,u} \qquad \forall i \in \mathcal{DG}, u \in \mathcal{U}, t \in \mathcal{T} \tag{4.23}$$

Finally, equations (4.24) and (4.25) represent active $p^{sh}_{i,u,t}$ and reactive $q^{sh}_{i,u,t}$ load shedding at each node, limited to the actual power demand, and follow the load power factor at each node ψ^d_i, as in (4.26).

$$p^{sh}_{i,u,t} \leq p^{d}_{i,u,t} \qquad \forall i \in \mathcal{B}, u \in \mathcal{U}, t \in \mathcal{T} \tag{4.24}$$

$$q^{sh}_{i,u,t} \leq q^{d}_{i,u,t} \qquad \forall i \in \mathcal{B}, u \in \mathcal{U}, t \in \mathcal{T} \tag{4.25}$$

$$q^{sh}_{i,u,t} = \sin(\cos^{-1}(\psi^d_i))\frac{p^{sh}_{i,u,t}}{\psi^d_i} \qquad \forall i \in \mathcal{B}, u \in \mathcal{U}, t \in \mathcal{T} \tag{4.26}$$

4.3. Investment Constraints

In order to model line investments, the proposed model considers binary and continuous variables. Binary variables represent whether the line is built or not, and continuous variables represent their capacity within specific bounds. The physical assets remain operational once installed, according to equations (4.27) and (4.28). The initially installed capacity is bounded by certain minimum and maximum magnitudes, in case the build decision is taken, as in equations (4.29) and (4.30).

$$x^{nf}_{ij,u-1} \leq x^{nf}_{ij,u} \qquad \forall ij \in \mathcal{L}, u \in \mathcal{U}, t \in \mathcal{T} \tag{4.27}$$

$$\rho^{nf}_{ij,u-1} \leq \rho^{nf}_{ij,u} \qquad \forall ij \in \mathcal{L}, u \in \mathcal{U}, t \in \mathcal{T} \tag{4.28}$$

$$\rho^{nf,\text{min}}_{ij} x^{nf}_{ij,u} \leq \rho^{nf}_{ij,u} \leq \rho^{nf,\text{max}}_{ij} x^{nf}_{ij,u} \qquad \forall ij \in \mathcal{L}, u \in \mathcal{U}, t \in \mathcal{T} \tag{4.29}$$

$$\rho^{nf}_{ij,u} - \rho^{nf}_{ij,u-1} \leq \rho^{nf,\text{max}}_{ij}(x^{nf}_{ij,u} - x^{nf}_{ij,u-1}) \qquad \forall ij \in \mathcal{L}, u \in \mathcal{U}, t \in \mathcal{T} \tag{4.30}$$

The same decision-making scheme rules the reinforcement of existent feeders as in equations (4.31)–(4.34). Finally, reinforcement decisions can only be taken one period

after the initial binary investment, as in (4.35).

$$x^{rf}_{ij,u-1} \leq x^{rf}_{ij,u} \qquad \forall ij \in \mathcal{L}, u \in \mathcal{U}, t \in \mathcal{T} \tag{4.31}$$

$$\rho^{rf}_{ij,u-1} \leq \rho^{rf}_{ij,u} \qquad \forall ij \in \mathcal{L}, u \in \mathcal{U}, t \in \mathcal{T} \tag{4.32}$$

$$\rho^{rf,\min}_{ij} x^{rf}_{ij,u} \leq \rho^{rf}_{ij,u} \leq \rho^{rf,\max}_{ij} x^{rf}_{ij,u} \qquad \forall ij \in \mathcal{L}, u \in \mathcal{U}, t \in \mathcal{T} \tag{4.33}$$

$$\rho^{rf}_{ij,u} - \rho^{rf}_{ij,u-1} \leq \rho^{rf,\max}_{ij}(x^{rf}_{ij,u} - x^{rf}_{ij,u-1}) \qquad \forall ij \in \mathcal{L}, u \in \mathcal{U}, t \in \mathcal{T} \tag{4.34}$$

$$x^{rf}_{ij,u} \leq x^{nf}_{ij,u-1} \qquad \forall ij \in \mathcal{L}, u \in \mathcal{U}, t \in \mathcal{T} \tag{4.35}$$

The same scheme applies to investments in new substations as in equations (4.36)–(4.39) and their reinforcement in constraints (4.40)–(4.43), given the temporal relation between these decisions as in (4.44).

$$z^{ns}_{i,u-1} \leq z^{ns}_{i,u} \qquad \forall i \in \mathcal{S}, u \in \mathcal{U}, t \in \mathcal{T} \tag{4.36}$$

$$\sigma^{ns}_{i,u-1} \leq \sigma^{ns}_{i,u} \qquad \forall i \in \mathcal{S}, u \in \mathcal{U}, t \in \mathcal{T} \tag{4.37}$$

$$\sigma^{ns,\min}_{i} z^{ns}_{i,u} \leq \sigma^{ns}_{i,u} \leq \sigma^{ns,\max}_{i} z^{ns}_{i,u} \qquad \forall i \in \mathcal{S}, u \in \mathcal{U}, t \in \mathcal{T} \tag{4.38}$$

$$\sigma^{ns}_{i,u} - \sigma^{ns}_{i,u-1} \leq \sigma^{ns,\max}_{i}(z^{ns}_{i,u} - z^{ns}_{i,u-1}) \qquad \forall i \in \mathcal{S}, u \in \mathcal{U}, t \in \mathcal{T} \tag{4.39}$$

$$z^{rs}_{i,u-1} \leq z^{rs}_{i,u} \qquad \forall i \in \mathcal{S}, u \in \mathcal{U}, t \in \mathcal{T} \tag{4.40}$$

$$\sigma^{rs}_{i,u-1} \leq \sigma^{rs}_{i,u} \qquad \forall i \in \mathcal{S}, u \in \mathcal{U}, t \in \mathcal{T} \tag{4.41}$$

$$\sigma^{rs,\min}_{i} z^{rs}_{i,u} \leq \sigma^{rs}_{i,u} \leq \sigma^{rs,\max}_{i} z^{rs}_{i,u} \qquad \forall i \in \mathcal{S}, u \in \mathcal{U}, t \in \mathcal{T} \tag{4.42}$$

$$\sigma^{rs}_{i,u} - \sigma^{rs}_{i,u-1} \leq \sigma^{rs,\max}_{i}(z^{rs}_{i,u} - z^{rs}_{i,u-1}) \qquad \forall i \in \mathcal{S}, u \in \mathcal{U}, t \in \mathcal{T} \tag{4.43}$$

$$z^{rs}_{i,u} \leq z^{ns}_{i,u-1} \qquad \forall i \in \mathcal{S}, u \in \mathcal{U}, t \in \mathcal{T} \tag{4.44}$$

In equation (4.45), investments in DG clusters are progressive, and these are bounded by a certain proportion β of the minimum load level at each bus, as in equation (4.46).

Total DG integration in the DN is also bounded by a proportion α of the minimum load level of the entire DN in (4.47).

$$\varphi^{dg}_{i,u-1} \leq \varphi^{dg}_{i,u} \qquad \forall i \in \mathcal{DG}, u \in \mathcal{U}, t \in \mathcal{T} \tag{4.45}$$

$$\varphi^{dg}_{i,u} \leq \beta p^{d}_{i,u,t} \qquad \forall i \in \mathcal{DG}, u \in \mathcal{U}, t \in \mathcal{T} \tag{4.46}$$

$$\sum_{i \in \mathcal{DG}} \varphi^{dg}_{i,u} \leq \alpha \sum_{i \in \mathcal{B}} p^{d}_{i,u,t} \qquad \forall u \in \mathcal{U}, t \in \mathcal{T} \tag{4.47}$$

4.4. Topology Constraints

Constraints (4.48)–(4.50) ensure the topology of the network remains radial, which is the case for several real-world DNs, and an assumption that strengthens the proposed linear relaxation of the power flows, as discussed in Section 3. Here, $n(\mathcal{B})$ and $n(\mathcal{B}^s)$ refer to the number of buses and substation buses, respectively. Also, constraints (4.51)–(4.54) prevent the planning of DG electrical islands, disconnected of all substations. These equations are based on Lavorato et al. (2012), and have been adapted to consider continuous capacity investments in DG clusters.

$$\sum_{i \in \mathcal{B}} \sum_{j \in \delta(i)} x^{nf}_{ij,u} = n(\mathcal{B}) - n(\mathcal{B}^s) - \sum_{i \in \Upsilon(u)} (1 - Y_{i,u}) \qquad \forall u \in \mathcal{U} \tag{4.48}$$

$$\sum_{j \in \delta(i)} x^{nf}_{ij,u} \geq 2Y_{i,u} \qquad \forall i \in \Upsilon(u), u \in \mathcal{U} \tag{4.49}$$

$$x^{nf}_{ij,u} \leq Y_{i,u} \qquad \forall ij \in \mathcal{L}, u \in \mathcal{U} \tag{4.50}$$

$$\mathcal{K}_{i,u} = \varphi^{dg}_{i,u} \qquad \forall i \in \mathcal{DG}, u \in \mathcal{U} \tag{4.51}$$

$$\mathcal{K}_{i,u} = 0 \qquad \forall i \notin (\mathcal{DG} \cup \mathcal{S}), u \in \mathcal{U} \tag{4.52}$$

$$\mathcal{K}_{i,u} = \sum_{j \in \delta(i)} \kappa_{ij,u} \qquad \forall i \in \mathcal{B}, u \in \mathcal{U} \tag{4.53}$$

$$|\kappa_{ij,u}| \leq \mathrm{M} x^{nf}_{ij,u} \qquad \forall ij \in \mathcal{L}, u \in \mathcal{U} \tag{4.54}$$

4.5. Nature of Variables

The nature of all variables, which completes the model, are presented up next.

$$x^{nf}_{ij,u}, x^{rf}_{ij,u} \in \{0,1\} \qquad \forall ij \in \mathcal{L}, u \in \mathcal{U} \tag{4.55}$$

$$z^{ns}_{i,u}, z^{rs}_{i,u}, Y_{i,u} \in \{0,1\} \qquad \forall i \in \mathcal{B}, u \in \mathcal{U} \tag{4.56}$$

$$\rho^{nf}_{ij,u}, \rho^{rf}_{ij,u} \geq 0 \qquad \forall ij \in \mathcal{L}, u \in \mathcal{U} \tag{4.57}$$

$$\sigma^{ns}_{i,u}, \sigma^{rs}_{i,u}, \varphi^{dg}_{i,u} \geq 0 \qquad \forall i \in \mathcal{B}, u \in \mathcal{U} \tag{4.58}$$

$$p^{s}_{i,u,t}, p^{dg}_{i,u,t}, p^{sh}_{i,u,t}, q^{sh}_{i,u,t} \geq 0 \qquad \forall i \in \mathcal{B}, u \in \mathcal{U}, t \in \mathcal{T} \tag{4.59}$$

4.6. Physical Validity Constraints

With all of the previous equations, we can formulate the DNP problem proposed in this thesis, through equations (4.1)–(4.59). In what follows, we strengthen this formulation by adding two types of physical validity constraints, with the purpose of improving the solving time of the problem.

First, the maximum active an reactive power losses are bounded by a proportion of the respective maximum transmission capacities η_{ij}, as in equations (4.60) and (4.61).

$$|p_{ij,u,t} + p_{ji,u,t}| \leq \eta_{ij}(\rho^{nf}_{ij,u} + \rho^{rf}_{ij,u}) \qquad \forall ij \in \mathcal{L}, u \in \mathcal{U}, t \in \mathcal{T} \tag{4.60}$$

$$|q_{ij,u,t} + q_{ji,u,t}| \leq \eta_{ij}(\rho^{nf}_{ij,u} + \rho^{rf}_{ij,u}) \qquad \forall ij \in \mathcal{L}, u \in \mathcal{U}, t \in \mathcal{T} \tag{4.61}$$

Second, we also know that power losses in the network are non-negative. Due to this, the following expression must be satisfied:

$$\sum_{i \in \mathcal{B}} \left(p^{s}_{i,u,t} + p^{dg}_{i,u,t} - p^{d}_{i,u,t} + p^{sh}_{i,u,t} \right) \geq 0 \qquad \forall u \in \mathcal{U}, t \in \mathcal{T} \tag{4.62}$$

$$\sum_{i \in \mathcal{B}} \left(q^{s}_{i,u,t} + q^{dg}_{i,u,t} - q^{d}_{i,u,t} + q^{sh}_{i,u,t} \right) \geq 0 \qquad \forall u \in \mathcal{U}, t \in \mathcal{T} \tag{4.63}$$

Even though the above equations (4.60)–(4.63) result redundant to the rest of the proposed DNP problem (4.1)–(4.58), and thus do not affect the solution space of the problem, they have the potential of significantly improving the efficiency of a mixed-integer optimization solver.

5. COMPUTATIONAL EXPERIMENTS

5.1. General Background

The proposed approach has been tested in a 13.8 kV, 24-node power distribution test system, which initial topology is shown in Figure 5.1, where existent assets are marked in solid lines, while candidate alternatives are presented in dashed lines. The detailed peak load and branch data can be found in Appendix B. The power factor was set to 0.93. The planning horizon is divided into three stages, each of which represents a five-year period, and considers a 5% discount rate and a capital recovery factor of 10% for all projects, for all of which a 25-year lifetime has been assumed. Upper and lower bounds for voltages at all nodes are set to 1.07 p.u. and 0.93 p.u.

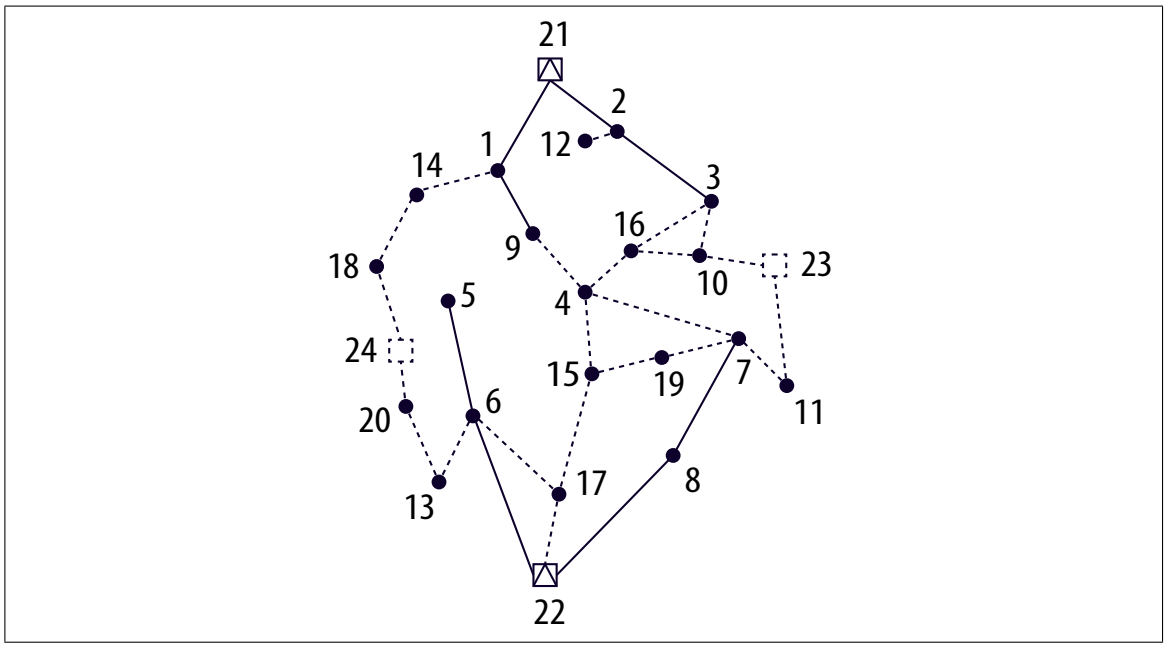

Figure 5.1. Initial topology of the 24-node power distribution test system. Adapted from Tabares et al. (2016)

The resistance and reactance of all branches are 0.40 Ω/km and 0.39 Ω/km, respectively. The capacity of existing branches is 5 MVA, while substations at bus 21 and 22

have initial capacities of 12 MVA and 15 MVA, respectively. Investment alternatives for existing and candidate feeders and substations are presented in Table 5.1, where all costs were adapted from Muñoz-Delgado et al. (2015). All buses are candidates for wind DG placement, for all of which a maximum hosting capacity $\beta = 250\%$ of their minimum load level has been set. Investment costs for wind DG is considered to be $1,700,000/MVA.

Table 5.1. Investment Data for Feeders and Substations

Element	Feeder		Substation	
Type	New	Reinf.	New	Reinf.
Min. Cap.	4 MVA	2 MVA	5 MVA	5 MVA
Max. Cap.	6 MVA	5 MVA	12 MVA	8 MVA
Fix. Cost	$2,000/km	$1,500/km	$150,000	$100,000
Var. Cost	$3,500/MVA·km	$3,000/MVA·km	$70,000/MVA	$70,000/MVA

All stages consider a representative year for their five-year period. Representative years are all equal for each stage and consider three load levels. These load blocks consider loading factors of 84%, 96% and 100% of the corresponding peak demand, and their durations are equal to 2,190 h/year, 5,475 h/year and 1,095 h/year, respectively. The capacity factor of wind DG at each load level is 36%, 32%, and 34%, respectively. The cost of purchasing power from the bulk power system at any substation, for each load block, is $58/MWh, $79/MWh, and $88/MWh, respectively. The cost for unserved energy υ_i^s is $2,000/MWh.

All experiments have been implemented in Python, and the Pyomo package, Hart et al. (2011)-Hart et al. (2017), was employed for optimization modeling. Gurobi, Gurobi Optimization (2016), was employed for solving mixed-integer optimization problems with an optimality gap of 1.0%, and IPOPT, Wächter & Biegler (2006), was employed for solving

non-convex AC-OPF problems. All experiments have been implemented in a Dell PowerEdge R360 server with an Intel Xeon CPU E5-2630 v4 processor running at 2.20GHz, and 64 GB of RAM.

We first study the potential of the model to assess the impact of the integration of DG into the expansion planning of the DN. We then evaluate the effectiveness and computational efficiency of the proposed model.

5.2. Impact of Distributed Energy Resources Integration

In this Section, we study the impact of DER integration using the proposed DNP model. Thus, three cases were studied: No Integration, Low Integration and High Integration of DERs. For each of these cases, the maximum systemic DG penetration level α was set to 0%, 100% and 200% of the minimum demand level. Parameters involved in the relaxations are selected as $\nu^{\alpha} = \nu^{\beta} = \nu^{\gamma} = 11$.

Figures 5.2, 5.3 and 5.4 show the DNP results across the planning horizon for cases with No Integration, Low Integration and High Integration of DERs, respectively. In these Figures, it can be observed how decisions change from one case to another based on the

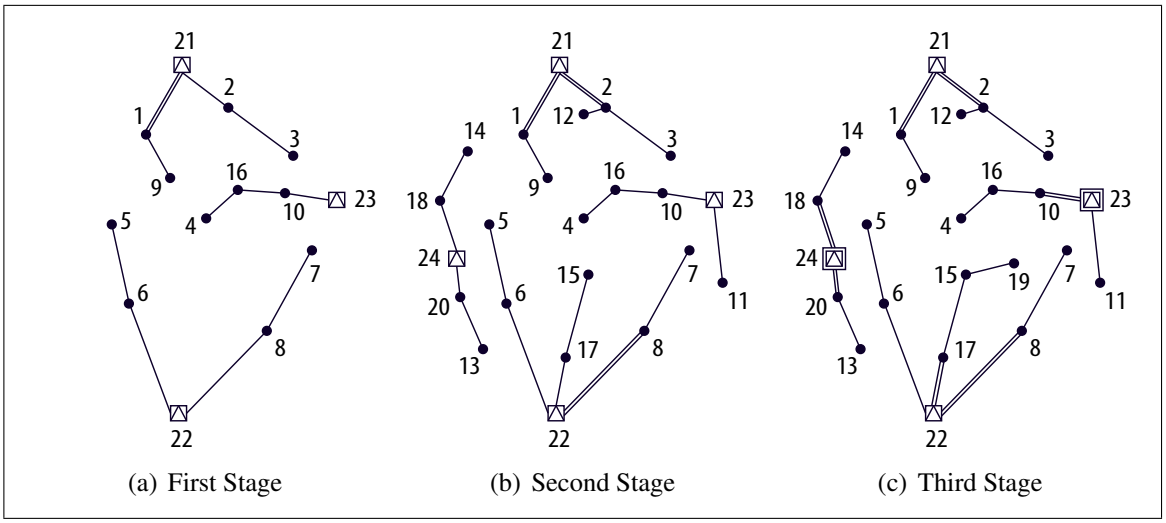

Figure 5.2. DNP Results for the No Integration Case

capacity of the DN to locally satisfy its energy demand, helping to avoid investments on feeders and substations.

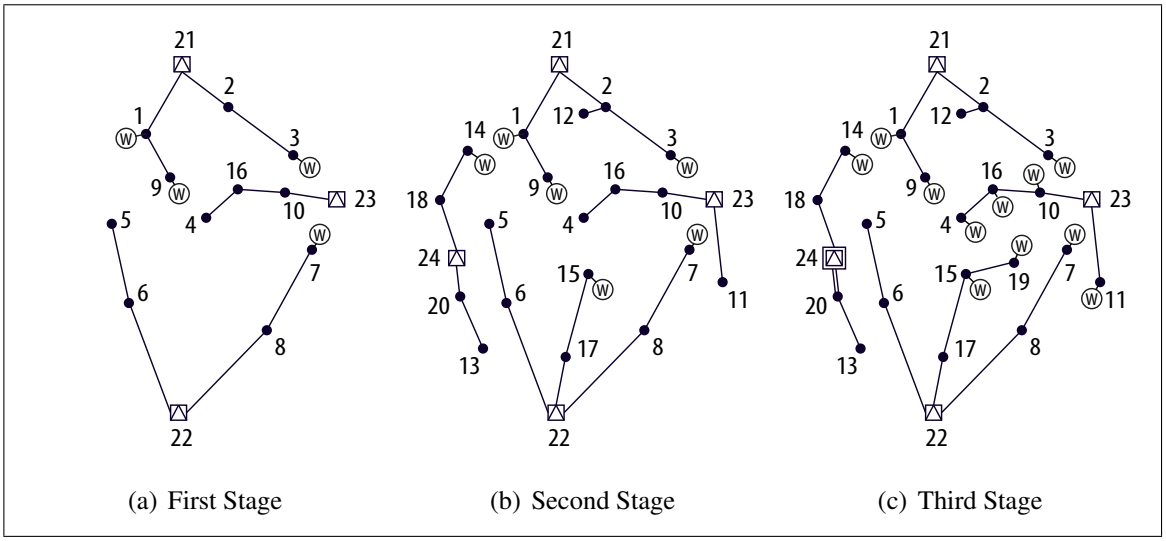

(a) First Stage (b) Second Stage (c) Third Stage

Figure 5.3. DNP Results for the Low Integration Case

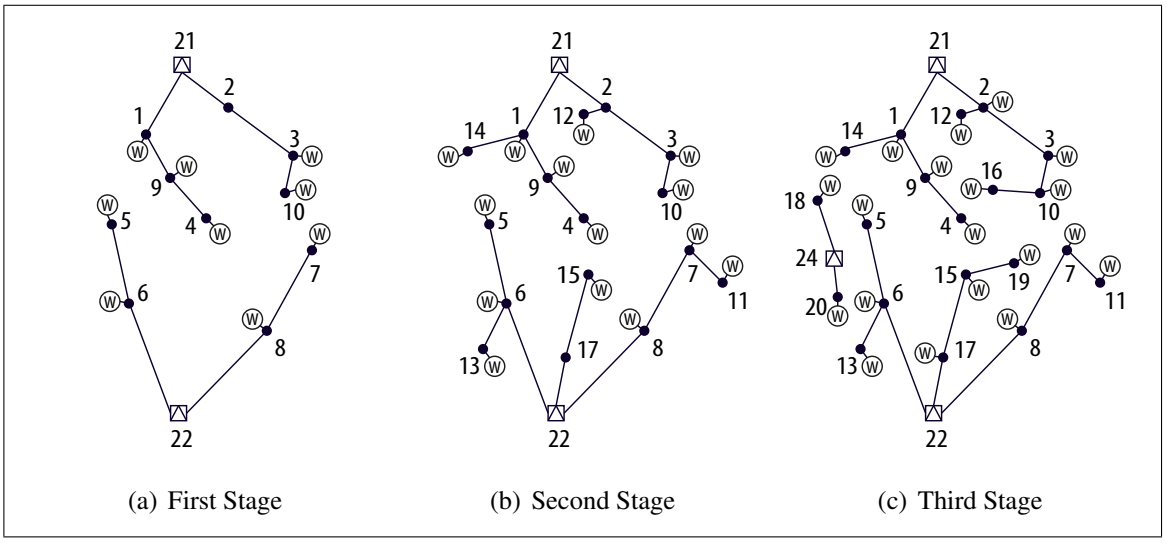

(a) First Stage (b) Second Stage (c) Third Stage

Figure 5.4. DNP Results for the High Integration Case

Figure 5.5 shows the net present cost structure breakdown for all cases. Here, FIC, SIC and DGIC refer to the total net present cost of all feeders, substations and DG clusters investments, respectively. OC corresponds to the net present cost of all operational costs through the planning horizon, and the sum of all of these concepts denotes the total net present cost (TNPC) of the DNP problem. In this Figure, we can observe how the TNPC under each case decreases as the maximum level of DG penetration increases, by drastically dropping the operational costs of the network by replacing the imports of energy from the bulk power system with DG injections, which also displaces and turns unnecessary further investments in distribution assets, consistent with what was observed in Figures 5.2, 5.3 and 5.4. Figure 5.5 data can be found in Table B.3.

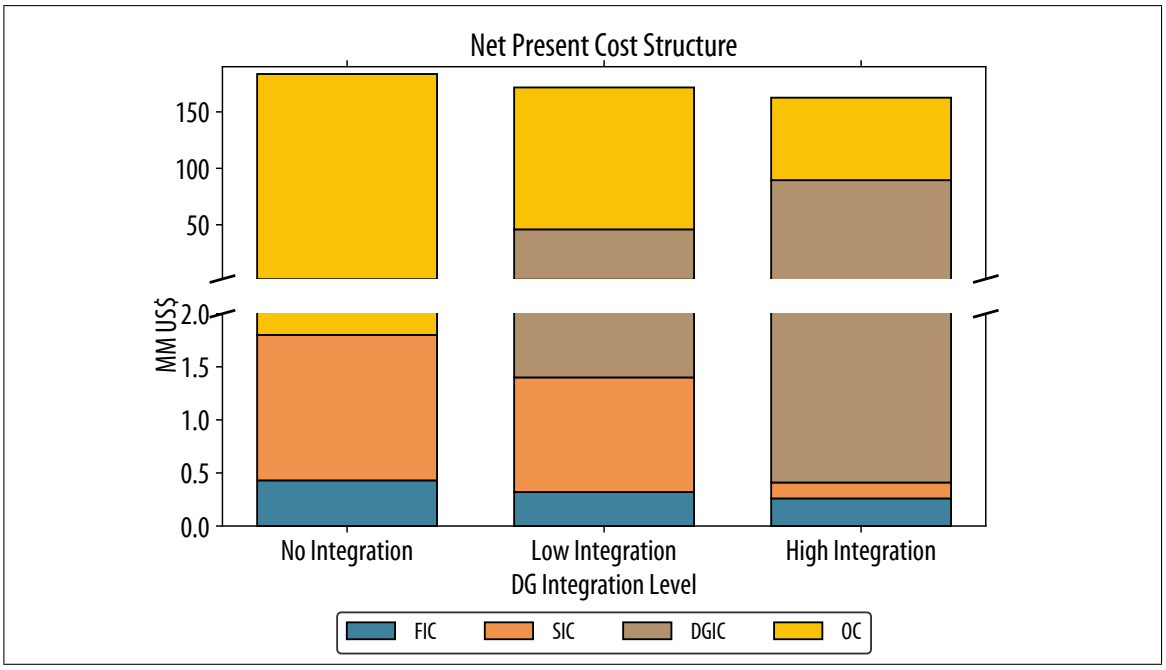

Figure 5.5. Net Present Cost Structure (MM US$)

As it can be noted, the progressive increase in the maximum level of DERs installation within the DN results in a larger renewable generation integration. For the No, Low and High Integration cases, the total renewable integration is 0%, 29.45% and 59.33%, respectively. Further, the reduction in power inflows from the bulk power system through the

DN also decreases power losses. As presented in Figure 5.6, for the case of active power losses across the planning horizon, these losses increased for the No Integration case from 3.8% in the first stage, up to 4.2% in the third stage. For the Low Integration case, they increased from 1.2% in the first stage, up to 1.5% in the final stage, while in the case of High Integration, losses rise from 0.5% at the beginning of the planning horizon, up to 0.7% at the end of it. The reduction in losses is a consequence of the reduction in power flows through the DN given the increase of on-site generation, which ultimately displaces the need of further distribution investments.

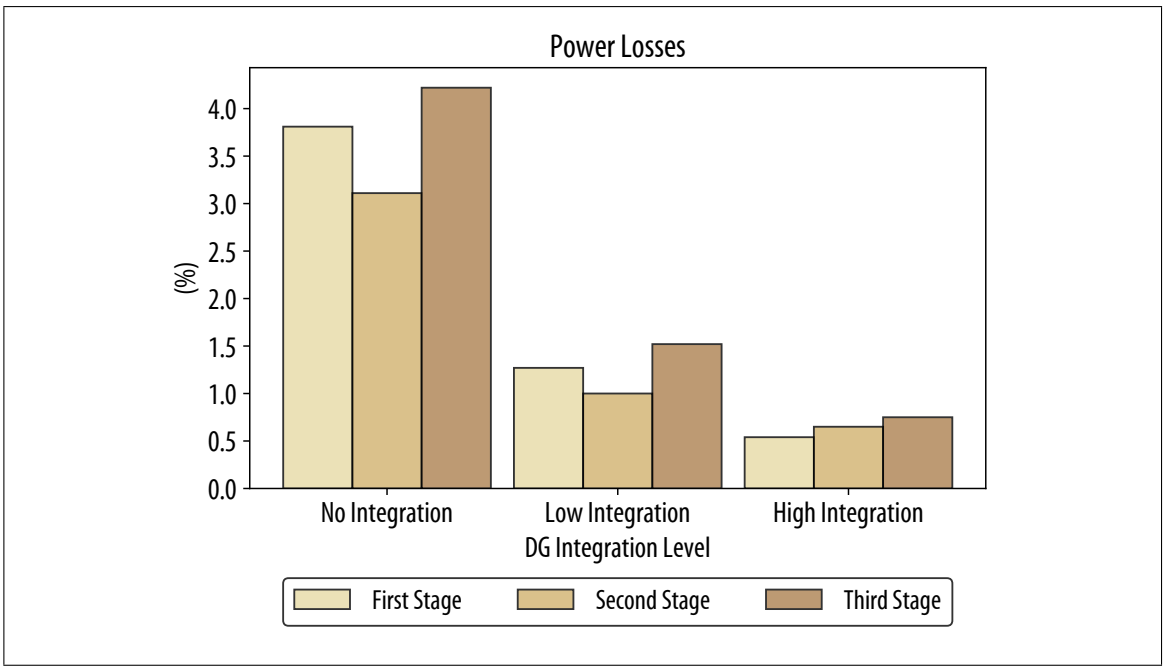

Figure 5.6. Solution Time for the Three Cases Studied Under Different Precision Parameters (Hours)

Note from the above analysis that the structure of the DNP model employed allows studying detailed power flow aspects such as power losses, as compared to simpler models that ignore some of such aspects. First, the LP-OPF within the DNP model explicitly considers voltages, reactive flows and losses. Such aspects would have not been represented by simpler models such as DC-OPF, which neglects voltage magnitudes, reactive

flows and losses, or other approximations solely based on Kirchhoff's Laws, for example, which completely obviates the relation between active and reactive power flows. Second, note that the fact that the DNP model proposed has a mixed-integer optimization structure implies that we do not need to rely in heuristics to solve the problem. Therefore, the proposed model combines an effective representation of the power flow equations, while also guaranteeing the quality of the DNP solution.

5.3. Accuracy and Efficiency of the Proposed Model

In what follows, Section 5.3.1 studies the quality and computational efficiency of the LP-OPF as a power flow model within DNP. Section 5.3.2 studies the improvements in computational tractability from considering the physical validity constraints in (4.60)–(4.63).

5.3.1. Precision and Efficiency of the LP-OPF in the DNP Problem

Recall from Sections 3 and 4 that the DNP model (4.1)–(4.63) is based in the LP-OPF in Model 3, which is a relaxation of SOCP-OPF in Model 2, which is itself a relaxation of AC-OPF in Model 1. Also, recall that parameter ν controls the tightness or precision of the polyhedral relaxation (4.17)–(4.19) of L^2, which is employed to construct the LP-OPF. This means that, the larger ν^α, ν^β and ν^γ are in the LP-OPF in Model 3, then, the closer the relaxation is to SOCP-OPF, and thus also to AC-OPF.

In order to study the effects of parameter ν, five experiments were conducted for each of the DG integration cases presented in Section 5.2. These experiments consider solving the DNP problem under $\nu = \nu^\alpha = \nu^\beta = \nu^\gamma$ set to 7, 9, 10, 11, and 12.

Figure 5.7 compares the power losses as represented by LP-OPF, as compared to the true power losses obtained from solving AC-OPF, under the respective DNP investment solutions obtained. It can be observed how the errors achieved by LP-OPF in representing

power losses increase sharply when reducing the precision parameter ν. Also, it is remarkable that these errors are less than 1% when ν is 11 or higher, under all the DG integration cases. Figure data can be found in Table B.4.

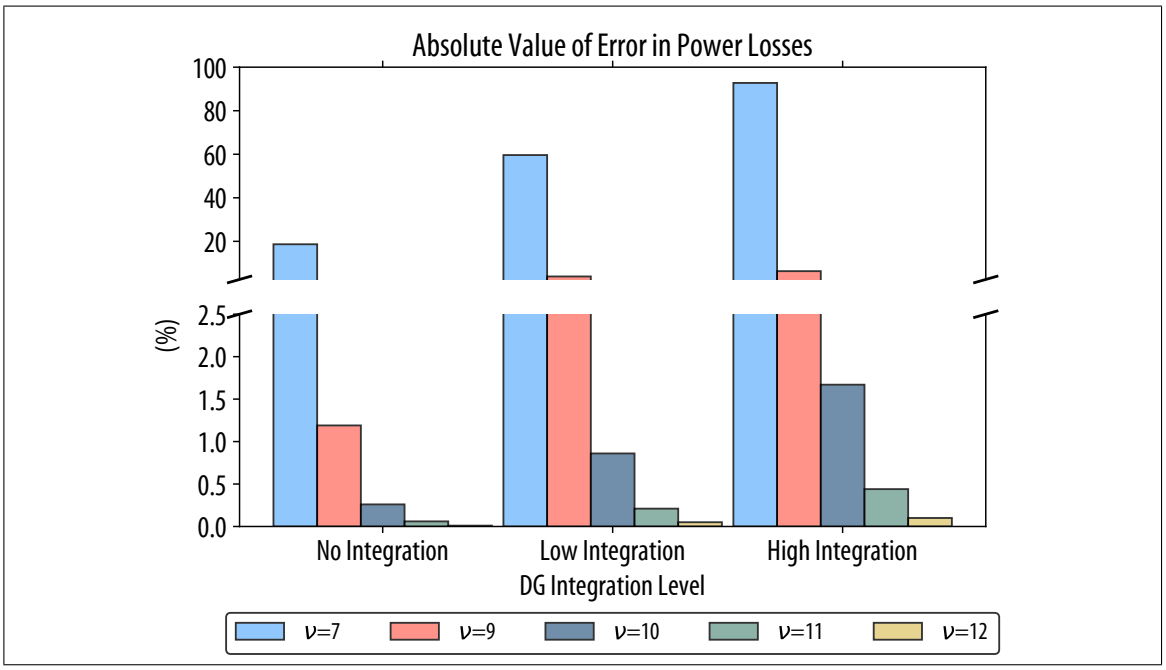

Figure 5.7. Error in Power Losses for the Three Cases Studied Under Different Precision Parameters (%)

Figure 5.8 shows the net present costs as represented by the DNP model (i.e. the objective value of problem (4.1)–(4.63)), and its associated costs overrun under AC-OPF, for all cases. Such cost under AC-OPF is calculated by fixing the investment solutions from the DNP model and solving the rest of the problem using AC-OPF equations. First, it can be observed that the costs based on LP-OPF increase as ν increases, which is to be expected since a smaller ν implies a more loose relaxation of the AC-OPF equations. Second, the costs overrun based on AC-OPF decrease as ν increases, and this is due to the fact that better investments solutions are obtained when the LP-OPF is a tighter approximation of the AC-OPF equations. Further, it is remarkable that the difference between the LP-OPF

and the AC-OPF planning costs are less than 0.01% when ν equals 11 and 12, which is consistent with the results in Figure 5.7. Figure data can be found in Table B.5.

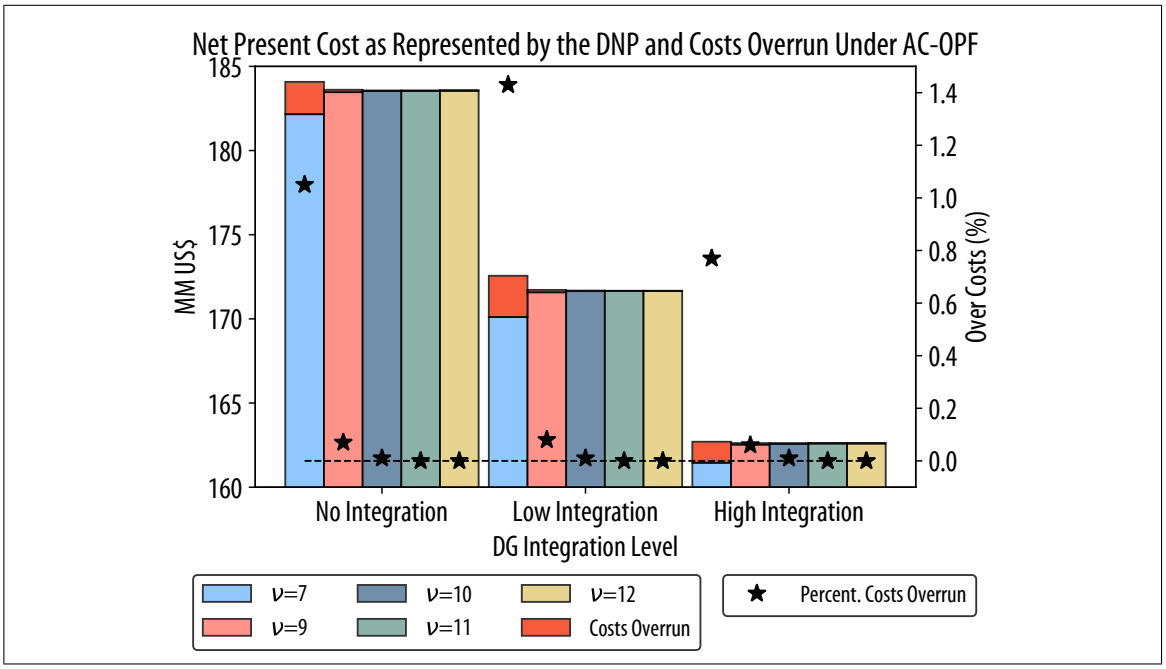

Figure 5.8. Total Net Present Cost (MM US$) as Represented by the DNP Model and its Comparison to the Associated Cost Under AC-OPF

Regarding the computational efficiency of the model, Figure 5.9 presents the solution time required to solve the DNP problem (4.1)–(4.63). We can observe that as the precision parameter ν increases, the solution times show a tendency to increase. This shows that there is an important tradeoff between computational efficiency and the quality of the solutions obtained. In this case study, a reasonable balance is achieved when $\nu = 11$. Figure data can be found in Table B.6.

All in all, these results show the trade-off between the effectiveness of the power flow relaxation and the computational tractability of the model. As it could be seen, decreasing the parameters involved in the LP-OPF results generally in lesser computational times yet in higher losses errors and total planning costs, as precision decreases. Nevertheless, a

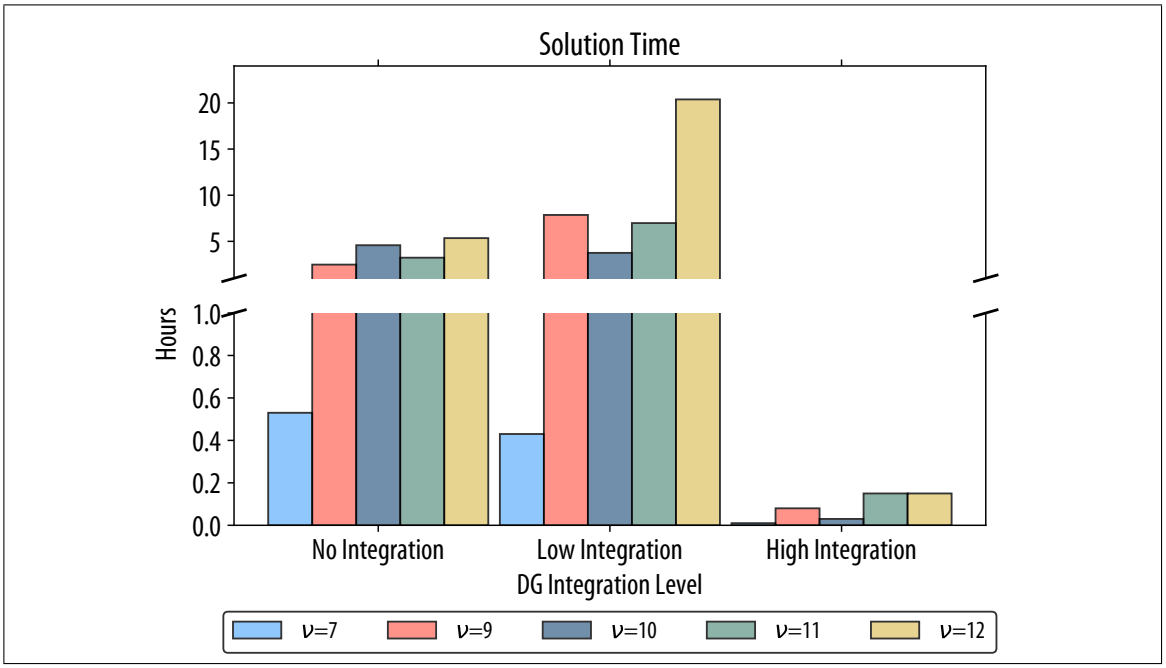

Figure 5.9. Solution Time for the Three Cases Studied Under Different Precision Parameters (Hours)

good balance is found between the computational efficiency of the model and an accurate representation of the PF equations when all parameters of construction of the linear relaxation are set equal to 11, which for all studied cases results in reasonable solving times without highly compromising the accuracy with respect to the AC-OPF, which is ultimately the reason why these values were considered for the cases presented in Section 5.2.

5.3.2. Impact of the Physical Validity Constraints

Finally, we study the computational efficiency of the DNP problem under the physical validity constraints (4.60)–(4.63). Figure 5.10 shows the solution time of the DNP problem under the presence and absence of these constraints. Here, “Min. Syst. Losses” refers to constraints (4.62) and (4.63), and “Max. Trans. Losses” refers to constraints (4.60) and (4.61). From this Figure we can first observe that if we ignore the two types of physical

validity constraints, the solution time becomes longer than 10 hours under all DG integration cases. As compared to this, adding any or both of the two types of physical validity constraints can significantly help in reducing the solve time. This shows the value of the physical validity constraints proposed to improve the tractability and practical application of the DNP model developed in this thesis. Finally, it is also important to note that the computational times achieved are reasonable for planning purposes. Figure data can be found in Table B.7.

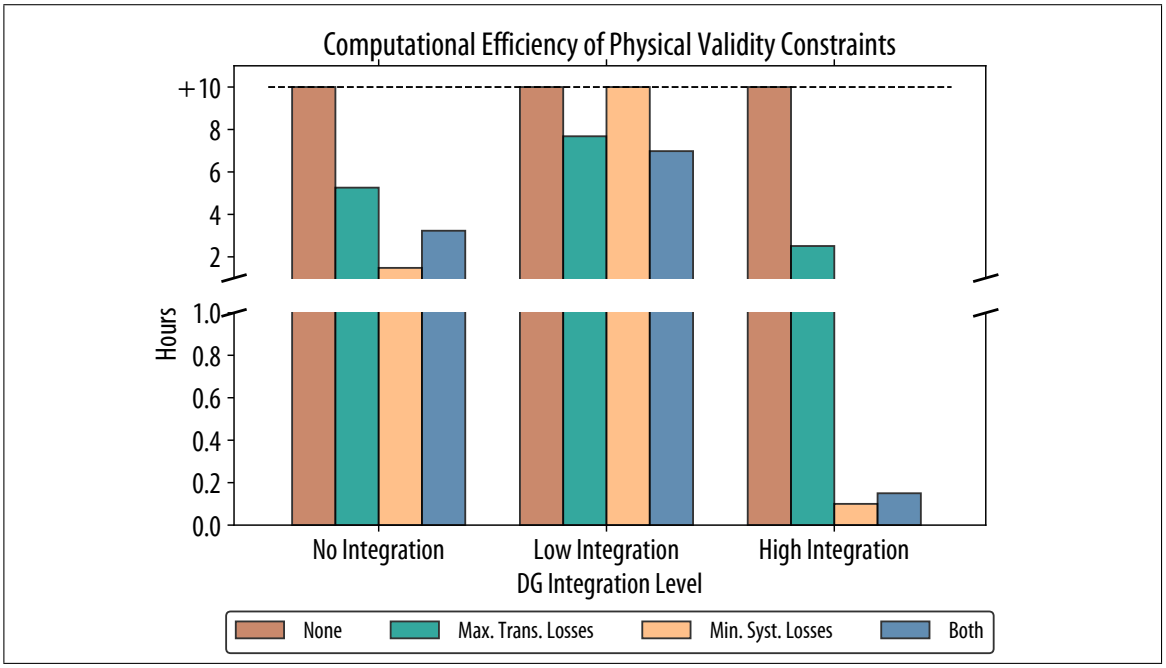

Figure 5.10. Computational Efficiency Of Physical Validity Constraints (Hours). "10+" Refers to a Solve Time Longer Than 10 Hours

Based on the experiments conducted in this Section, it can be noted that under the proposed approach, for all studied cases, the total cost of the operation and expansion planning of the DN differs in less than 0.01% from the actual costs when operation is subject to an AC-OPF model, which results specially relevant to a distribution system operator that has to face a surge in DERs integration. Further, the model reliably combines

an effective representation of the PF equations, while guaranteeing the optimality of its solution within a 1% optimality gap.

In summary, this Section has shown the value of the proposed approach in analyzing DERs integration, the effectiveness of LP-OPF as a power flow model in the DNP problem, and the practical computational tractability of the model.

6. CONCLUDING REMARKS AND FUTURE WORK

This thesis developes a mixed-integer optimization model for the DNP problem that accurately represents the physics of power flows through a tight polyhedral relaxation of the power flow equations. Exploiting this relaxation the proposed DNP model is capable of assessing the optimal allocation, sizing and timing of new investments and reinforcements in capacity of not only feeders and substations, but also DG clusters within the DN. Thus, harnessing the benefits of DERs while facing the challenges of its, in otherwise, unplanned integration, which is envisioned as a key role of modern distribution system operators.

Extensive experiments assess the effectiveness and the computational tractability of this approach. Based on these results, the proposed model shows an effective representation of the AC power flow equations, while also guaranteeing the quality of the DNP solution. Additionally, although there is an important tradeoff between computational efficiency and the quality of the solutions obtained, it is important to note that physical validity constraints can significantly improve the solving times, and thus, a practical computational tractability of the model for planning purposes.

Many directions of future work are open. First, it would be desirable to incorporate some relevant features that have not been considered in the proposed approach to the DNP problem. On the one hand, and regarding the accuracy of the proposed model to represent elements of the power flow equations, the modelling of capacitor banks and voltage regulators would exploit the effectiveness of the model to leverage their impact in the planning and operational decisions. On the other hand, the optimal integration of other DERs such as other renewable or conventional DG units, electric vehicles, battery energy storage systems, and demand response programs, is also expected to help displace the need for further distribution investments.

Second, it is relevant to perform additional analysis to understand the value of the additional physical validity constraints and their impact in the solving time of the problem. In this line, it would be of interest to tighten these constraints by reducing the maximum

proportion of losses η_{ij}, given the maximum transmission capacity between nodes i and j, in equations (4.60) and (4.61), and by introducing a minimum percentage of systemic power losses, given the maximum systemic DG penetration level α, in equations (4.62) and (4.63), which would need a deeper understanding of the power flows phenomena within the studied DN, in order to prevent modifications in the optimal solution of the problem. All in all, it is expected that tighter physical validity constraints would further reduce the solving time of the problems as presented in Figure 5.10.

REFERENCES

Alotaibi, M. A., & Salama, M. (2018). An incentive-based multistage expansion planning model for smart distribution systems. *IEEE Trans. Power Syst.*, *PP*(99), 1-1.

Asensio, M., de Quevedo, P. M., Munoz-Delgado, G., & Contreras, J. (2016a). Joint distribution network and renewable energy expansion planning considering demand response and energy storage; part ii: Numerical results and considered metrics. *IEEE Transactions on Smart Grid*, *PP*(99), 1-1.

Asensio, M., de Quevedo, P. M., Munoz-Delgado, G., & Contreras, J. (2016b). Joint distribution network and renewable energy expansion planning considering demand response and energy storage; part i: Stochastic programming model. *IEEE Transactions on Smart Grid*, *PP*(99), 1-1.

Bai, X., Wei, H., Fujisawa, K., & Wang, Y. (2008). Semidefinite programming for optimal power flow problems. *International Journal of Electrical Power & Energy Systems*, *30*(6-7), 383–392.

Ben-Tal, A., & Nemirovski, A. (2001). On polyhedral approximations of the second-order cone. *Mathematics of Operations Research*, *26*(2), 193-205. Retrieved from `http://www.jstor.org/stable/3690614`

Coffrin, C., Hijazi, H. L., & Van Hentenryck, P. (2016). The qc relaxation: A theoretical and computational study on optimal power flow. *IEEE Trans. Power Syst.*, *31*(4), 3008–3018.

Coffrin, C., & Van Hentenryck, P. (2014). A linear-programming approximation of ac power flows. *INFORMS Journal on Computing*, *26*(4), 718–734.

El-Khattam, W., & Salama, M. (2004). Distributed generation technologies, definitions and benefits. *Electric Power Systems Research*, *71*(2), 119 - 128. Retrieved from http://www.sciencedirect.com/science/article/pii/S0378779604000240

Gönen, T., & Foote, B. L. (1981, March). Distribution-system planning using mixed-integer programming. *IEE Proceedings C - Generation, Transmission and Distribution*, *128*(2), 70-79.

Gurobi Optimization, I. (2016). *Gurobi optimizer reference manual.* Retrieved from http://www.gurobi.com

Haffner, S., Pereira, L. F. A., Pereira, L. A., & Barreto, L. S. (2008a, April). Multistage model for distribution expansion planning with distributed generation; part ii: Numerical results. *IEEE Trans. Power Del.*, *23*(2), 924-929.

Haffner, S., Pereira, L. F. A., Pereira, L. A., & Barreto, L. S. (2008b, April). Multistage model for distribution expansion planning with distributed generation; part i: Problem formulation. *IEEE Trans. Power Del.*, *23*(2), 915-923.

Hart, W. E., Laird, C. D., Watson, J.-P., Woodruff, D. L., Hackebeil, G. A., Nicholson, B. L., & Siirola, J. D. (2017). *Pyomo–optimization modeling in python* (Second ed., Vol. 67). Springer Science & Business Media.

Hart, W. E., Watson, J.-P., & Woodruff, D. L. (2011). Pyomo: modeling and solving mathematical programs in python. *Mathematical Programming Computation*, *3*(3), 219–260.

Jabr, R. (2012). Tight polyhedral approximation for mixed-integer linear programming unit commitment formulations. *IET Generation, Transmission & Distribution*, *6*(11), 1104–1111.

Jabr, R. A. (2006). Radial distribution load flow using conic programming. *IEEE Trans. Power Syst.*, *21*(3), 1458–1459.

Jabr, R. A. (2008). Optimal power flow using an extended conic quadratic formulation. *IEEE Trans. Power Syst.*, *23*(3), 1000–1008.

Keane, A., Ochoa, L. F., Borges, C. L. T., Ault, G. W., Alarcon-Rodriguez, A. D., Currie, R. A. F., ... Harrison, G. P. (2013, May). State-of-the-art techniques and challenges ahead for distributed generation planning and optimization. *IEEE Trans. Power Syst.*, *28*(2), 1493-1502.

Kocuk, B., Dey, S. S., & Sun, X. A. (2016a, Jan). Inexactness of sdp relaxation and valid inequalities for optimal power flow. *IEEE Trans. Power Syst.*, *31*(1), 642-651.

Kocuk, B., Dey, S. S., & Sun, X. A. (2016b). Strong socp relaxations for the optimal power flow problem. *Operations Research*, *64*(6), 1177–1196.

Kocuk, B., Dey, S. S., & Sun, X. A. (2017). New formulation and strong misocp relaxations for ac optimal transmission switching problem. *IEEE Trans. Power Syst.*, *32*(6), 4161–4170.

Koutsoukis, N. C., Georgilakis, P. S., & Hatziargyriou, N. D. (2018). Multistage coordinated planning of active distribution networks. *IEEE Trans. Power Syst.*, *33*(1), 32–44.

Lavaei, J., & Low, S. H. (2012, Feb). Zero duality gap in optimal power flow problem. *IEEE Trans. Power Syst.*, *27*(1), 92-107.

Lavorato, M., Franco, J. F., Rider, M. J., & Romero, R. (2012, Feb). Imposing radiality constraints in distribution system optimization problems. *IEEE Trans. Power Syst.*, *27*(1), 172-180.

Low, S. H. (2014a, March). Convex relaxation of optimal power flowpart i: Formulations and equivalence. *IEEE Transactions on Control of Network Systems*, *1*(1), 15-27.

Low, S. H. (2014b, June). Convex relaxation of optimal power flowpart ii: Exactness. *IEEE Transactions on Control of Network Systems*, *1*(2), 177-189.

Muñoz-Delgado, G., Contreras, J., & Arroyo, J. M. (2015, July). Joint expansion planning of distributed generation and distribution networks. In *2015 ieee power energy society general meeting* (p. 1-1).

Paliwal, P., Patidar, N., & Nema, R. (2014). Planning of grid integrated distributed generators: A review of technology, objectives and techniques. *Renewable and Sustainable Energy Reviews*, *40*, 557 - 570. Retrieved from `http://www.sciencedirect.com/science/article/pii/S1364032114006601`

Pepermans, G., Driesen, J., Haeseldonckx, D., Belmans, R., & D'haeseleer, W. (2005). Distributed generation: definition, benefits and issues. *Energy Policy*, *33*(6), 787 - 798. Retrieved from `http://www.sciencedirect.com/science/article/pii/S0301421503003069`

Prakash, P., & Khatod, D. K. (2016). Optimal sizing and siting techniques for distributed generation in distribution systems: A review. *Renewable and Sustainable Energy Reviews*, *57*(Supplement C), 111 - 130. Retrieved from `http://www.sciencedirect.com/science/article/pii/S1364032115014823`

Pudjianto, D., Ramsay, C., & Strbac, G. (2007, March). Virtual power plant and system integration of distributed energy resources. *IET Renewable Power Generation*, *1*(1), 10-16.

Shen, X., Shahidehpour, M., Han, Y., Zhu, S., & Zheng, J. (2017, Jan). Expansion planning of active distribution networks with centralized and distributed energy storage systems. *IEEE Transactions on Sustainable Energy*, *8*(1), 126-134.

Tabares, A., Franco, J. F., Lavorato, M., & Rider, M. J. (2016, May). Multistage long-term expansion planning of electrical distribution systems considering multiple alternatives. *IEEE Trans. Power Syst.*, *31*(3), 1900-1914.

Theo, W. L., Lim, J. S., Ho, W. S., Hashim, H., & Lee, C. T. (2017). Review of distributed generation (dg) system planning and optimisation techniques: Comparison of numerical and mathematical modelling methods. *Renewable and Sustainable Energy Reviews*, *67*(Supplement C), 531 - 573. Retrieved from `http://www.sciencedirect.com/science/article/pii/S1364032116305421`

Vielma, J. P., Ahmed, S., & Nemhauser, G. L. (2008). A lifted linear programming branch-and-bound algorithm for mixed-integer conic quadratic programs. *INFORMS Journal on Computing*, *20*(3), 438–450.

Wächter, A., & Biegler, L. T. (2006). On the implementation of an interior-point filter line-search algorithm for large-scale nonlinear programming. *Mathematical programming*, *106*(1), 25–57.

Zeng, B., Zhang, J., Yang, X., Wang, J., Dong, J., & Zhang, Y. (2014, May). Integrated planning for transition to low-carbon distribution system with renewable energy generation and demand response. *IEEE Trans. Power Syst.*, *29*(3), 1153-1165.

Ziari, I., Ledwich, G., & Ghosh, A. (2013, July). Optimal distribution network reinforcement considering load growth, line loss and reliability. In *2013 ieee power energy society general meeting* (p. 1-1).

APPENDICES

A. POLYHEDRAL APPROXIMATION OF THE LORENTZ CONE

Following Ben-Tal & Nemirovski (2001), it can be shown that the Lorentz cone

$$\mathrm{L}^2 = \left\{ \left(\alpha, \beta, \gamma\right) \middle| \sqrt{y_1^2 + y_2^2} \leq y_3 \right\} \tag{a}$$

Can be approximated as follows:

$$\varpi^0 \geq |y_1| \tag{b1}$$

$$\varrho^0 \geq |y_2| \tag{b2}$$

$$\varpi^k = \cos\left(\frac{\pi}{2^{k+1}}\right)\varpi^{k-1} + \sin\left(\frac{\pi}{2^{k+1}}\right)\varrho^{k-1} \quad k = 1...\nu \tag{b3}$$

$$\varrho^k \geq |-\sin\left(\frac{\pi}{2^{k+1}}\right)\varpi^{k-1} + \cos\left(\frac{\pi}{2^{k+1}}\right)\varrho^{k-1}| \; k = 1...\nu \tag{b4}$$

$$\varpi^\nu \leq y_3 \tag{b5}$$

$$\varrho^\nu \leq \tan\left(\frac{\pi}{2^{\nu+1}}\right)\varpi^\nu \tag{b6}$$

Here, (b) is a system of linear homogeneous inequalities that form a space denoted by $\mathcal{P}^\nu(y_1, y_2, y_3, \boldsymbol{\mu}) \geq 0$. Where $\boldsymbol{\mu}$ is the collection of the $2(\nu + 1)$ variables ϖ^k and ϱ^k, for $k = 0, \ldots, \nu$, and the positive integer ν is a parameter of construction of the approximation. Refer to Ben-Tal & Nemirovski (2001) for a better understanding on this approximation.

B. COMPUTATIONAL EXPERIMENTS

B.1. General Background

Table B.1. Lines Data. Adapted from Tabares et al. (2016)

Line	From i bus	To j bus	Length (km)	Line	From i bus	To j bus	Length (km)
1	1	9	2.100	16	6	22	4.550
2	1	14	2.100	17	7	8	3.500
3	1	21	3.850	18	7	11	1.925
4	2	3	3.500	19	7	19	2.800
5	2	12	1.925	20	8	22	3.500
6	2	21	2.975	21	10	16	1.400
7	3	10	1.925	22	10	23	2.275
8	3	16	2.100	23	11	23	2.800
9	4	7	4.550	24	13	20	2.100
10	4	9	2.100	25	14	18	1.750
11	4	15	2.800	26	15	17	2.100
12	4	16	2.275	27	15	19	2.800
13	5	6	4.200	28	17	22	2.625
14	6	13	2.100	29	18	24	2.625
15	6	17	3.850	30	20	24	1.575

Table B.2. Peak Load Data (MVA). Adapted from Tabares et al. (2016)

Bus	Stage			Bus	Stage		
	1	2	3		1	2	3
1	4.05	3.45	5.42	11	0.00	1.91	2.80
2	0.78	0.77	1.21	12	0.00	0.93	1.29
3	2.58	3.38	3.98	13	0.00	1.15	1.87
4	0.32	0.41	2.43	14	0.00	3.05	3.16
5	0.28	0.37	0.47	15	0.00	1.62	1.62
6	1.17	0.92	1.81	16	0.00	0.00	1.22
7	4.04	3.70	4.36	17	0.00	2.16	2.40
8	0.72	0.60	0.94	18	0.00	0.00	2.10
9	1.14	1.12	1.77	19	0.00	0.00	1.81
10	1.56	2.04	2.40	20	0.00	0.00	3.79

B.2. Impact of Distributed Energy Resources Integration

Table B.3. Net Present Cost Structure (MM US$)

Item	No Integration	Low Integration	High Integration
FIC	0.43	0.32	0.26
SIC	1.37	1.08	0.15
DGIC	0	44.56	89.13
OC	181.74	125.67	73.04
TNPC	183.55	171.66	162.60

B.3. Accuracy and Efficiency of the Proposed Model

B.3.1. Precision and Efficiency of the LP-OPF in the DNP Problem

Table B.4. Error in Power Losses for the Three Cases Studied Under Different Precision Parameters (%)

Precision Parameter	No Integration	Low Integration	High Integration
12	-0.01	-0.05	-0.10
11	-0.06	-0.21	-0.44
10	-0.26	-0.86	-1.67
9	-1.19	-3.87	-6.31
7	-18.66	-59.63	-92.76

Table B.5. Total Net Present Cost (MM US$) as Represented by the DNP Model and its Comparison to the Associated Cost Under AC-OPF

Case	No Integration			Low Integration			High Integration		
Prec. Param.	DNP	AC-OPF	Diff. (%)	DNP	AC-OPF	Diff. (%)	DNP	AC-OPF	Diff. (%)
12	183.56	183.56	0.00	171.66	171.67	0.00	162.60	162.60	0.00
11	183.55	183.56	0.00	171.66	171.67	0.00	162.60	162.60	0.00
10	183.54	183.57	0.01	171.65	171.68	0.01	162.58	162.61	0.01
9	183.47	183.61	0.07	171.58	171.72	0.08	162.53	162.64	0.06
7	182.16	184.08	1.05	170.11	172.56	1.43	161.45	162.70	0.77

Table B.6. Solution Time for the Three Cases Studied Under Different Precision Parameters (Hours)

Precision Parameter	No Integration	Low Integration	High Integration
12	5.35	20.38	0.15
11	3.23	6.98	0.15
10	4.58	3.75	0.03
9	2.48	7.86	0.08
7	0.53	0.43	0.01

B.3.2. Impact of the Physical Validity Constraints

Table B.7. Computational Efficiency Of Physical Validity Constraints (Hours). "10+" Refers to a Solve Time Longer Than 10 Hours

Min. Syst. Losses	Max. Trans. Losses	No Integration	Low Integration	High Integration
✓	✓	3.23	6.98	0.15
✓	✗	1.48	10+	0.10
✗	✓	5.26	7.68	2.51
✗	✗	10+	10+	10+